Bioprinting in granular support hydrogels - characterizing the role of particle morphology and packing density

Graham Britchfield [1], Andrew Daly [1,2,*]

[1] Biomedical Engineering, National University of Ireland Galway, Galway, Ireland

[2] CÚRAM, SFI Research Centre for Medical Devices, National University of Ireland Galway, Galway, Ireland

*email: andrew.daly@nuigalway.ie

Abstract

Embedded bioprinting into support hydrogels enables controlled extrusion of low viscosity bioinks into complex 3D structures with high-resolution features. Granular hydrogels, formed through packing of hydrogel microparticles, are increasingly employed as support materials due to their shear-thinning and self-healing properties that are essential for the embedded bioprinting process. Despite the widespread use of granular support hydrogels for embedded bioprinting, their general design criteria such as the optimal particle morphology, size, and packing density have not been established. Here, we developed granular support hydrogels with varied particle morphologies and packing densities, to explore how these parameters can influence rheological behaviour and the embedded bioprinting process. Interestingly, lower viscosity support hydrogels with a higher yield point, formulated from particles with irregular morphologies that increased particle-particle interactions, were found to improve print quality outcomes. In particular, we observed these formulations improved extrusion consistency during complex print paths and reduced disruption of adjacent filaments during successive print paths. These results improve our understanding of particle-particle interactions in granular support hydrogels during embedded bioprinting, and can be used to inform the design of future support hydrogel compositions.

Introduction

A major challenge in bioprinting has been developing bioinks that possess high levels of manufacturability and that simultaneously mimic the structure of the extracellular matrix (ECM)[1–3]. As a result, an increasingly common approach involves bioprinting in support hydrogels where the bioink is extruded into a soft hydrogel that provides support to maintain filament fidelity both during and after extrusion [4,5]. For example, support hydrogels have enabled high fidelity bioprinting with low viscosity bioinks such as collagen that are otherwise challenging to process using traditional extrusion onto a flat two-dimensional surface [6,7]. This has significantly expanded the number of hydrogels compatible with extrusion bioprinting, and enabled processing of lower density hydrogel compositions that are required to promote cellular processes such as proliferation, differentiation, and ECM production [1,8]. For example, extrusion of collagen bioinks into support hydrogels has been used to bioprint anatomically accurate components of the human heart including contractile ventricles and heart valves [9].

Support hydrogels fabricated using jammed hydrogel microparticles are increasingly used due to their shear-thinning and self-healing properties, along with their relative ease of fabrication [10–12]. The earliest particle based support hydrogels were fabricated using gelatin microparticles, now commonly referred to as FRESH (freeform reversible embedding of suspended hydrogels)[11]. Several other groups have also developed particle based support hydrogels using agarose, polyacrylamide, and alginate [7,10,11,13–15]. Interestingly, despite the increasing use of particle-based support hydrogels, general design criteria for their development have not yet been established. For example, a wide variety of manufacturing methods are used to create microparticles for granular hydrogels, which can result in significant differences in their rheological behaviour,

along with the morphology of the particles themselves [16–18]. It has been demonstrated that increases in support hydrogel viscosity can improve print resolution, measured by quantifying the width of extruded filaments [9,14,19]. Similarly, lower viscosity in granular support hydrogels has been shown cause greater filament instability and buckling during deposition, particularly when the extrusion and nozzle translation speeds are not matched [19]. However, it is not well understood how specific rheological parameters, driven by particle-particle interactions, can influence many print quality outcomes - particularly beyond relatively simple outcomes such as the diameter of extruded beams. For example, the fluidic behaviour of the support hydrogel will significantly impact complex aspects of the printing process such direction changes and the disruption of previously deposited ink during successive deposition steps. This paper aims to address this gap in knowledge by developing support hydrogels with a wide range of particle morphologies and rheological properties, and then establishing how varying these parameters can influence print quality outcomes during embedded bioprinting.

Main

Development and rheological characterization of granular support hydrogels with varied particle morphology and density

First, we developed agarose microgels using a shearing method that has been widely used for creating granular support hydrogels [14,20,21]. By varying the agarose polymer concentration during shearing we observed distinct differences in particle morphology (Fig 1a). The particles broadly share an overall structure - a central mass making up the majority of the body, with elongated protrusions extending from this body (Fig 1a). However, we observed pronounced differences in the size of the particle body, protrusion number, and protrusion length as the polymer concentration was varied (Fig 1 b-d). For example, the particle diameter decreased with increasing polymer concentration (Fig 1b). Similarly, the protrusion length decreased with increasing polymer concentration (Fig 1d). The most striking difference in particle morphology was the number of protrusions exhibited across the different polymer concentrations, with significant increases observed at 0.5% (Fig 1c). These particle morphologies have been reported before, and are thought to be caused by temperature gradients that arise as shear is applied to the material as it crosslinks during cooling [16,17]. As these protrusions will alter particle-particle interactions in a jammed formulation, we next sought to characterize changes in rheological properties with varied particle morphology and packing density.

Viscosity sweeps at increasing shear rate demonstrated that in jammed formulations all particle morphologies produced hydrogels with shear-thinning properties (Fig 2a). Increases in viscosity were observed for 2% particles, likely due to the increased stiffness of the hydrogel network itself at higher polymer concentrations. Thixotropic tests demonstrated all support hydrogel formulations had self-healing properties as the viscosity recovered through periods of low and high strain (Fig 2b). Interestingly, viscosity values increased following a cycle of high strain across all formulations, potentially related to increased particle interactions and entanglements following shear disruption. Finally, using strain sweeps we characterized how the relative elastic and viscous properties varied depending on the deformation rate. Storage and loss modulus values increased with increasing polymer concentration (Fig 2c), and the yield point, defined as the storage and loss modulus crossover, was found to decrease with increasing polymer concentration (Fig 2d). This indicated that support hydrogels created using the 2% agarose particles displayed more viscous behaviour at lower strain values. A potential factor here is entanglement of particle protrusions. Due to this entanglement, increased shear may be required to initiate flow leading to a higher yield point.

The increases in viscosity and storage modulus values that were observed for higher polymer concentration particles may also be a result of the increased densification of jammed particles containing a lower number of protrusions. To test this hypothesis, we compared the rheological properties of microparticles with and without particle protrusions. To do this, we used an emulsion technique to create spherical agarose microparticles containing no protrusions, and then compared their rheological properties to particles of the same mean diameter containing protrusions (produced using shearing) (Fig 2e). Rheological characterization of the two groups in a jammed hydrogel formulation

demonstrated an increase in viscosity with the presence of particle protrusions (Fig 2f). Similarly, in strain sweep tests, a significant increase in the yield point was observed (Fig 2f). This indicates that the presence of protrusions that increase particle-particle interactions can alter the rheological properties of granular hydrogels.

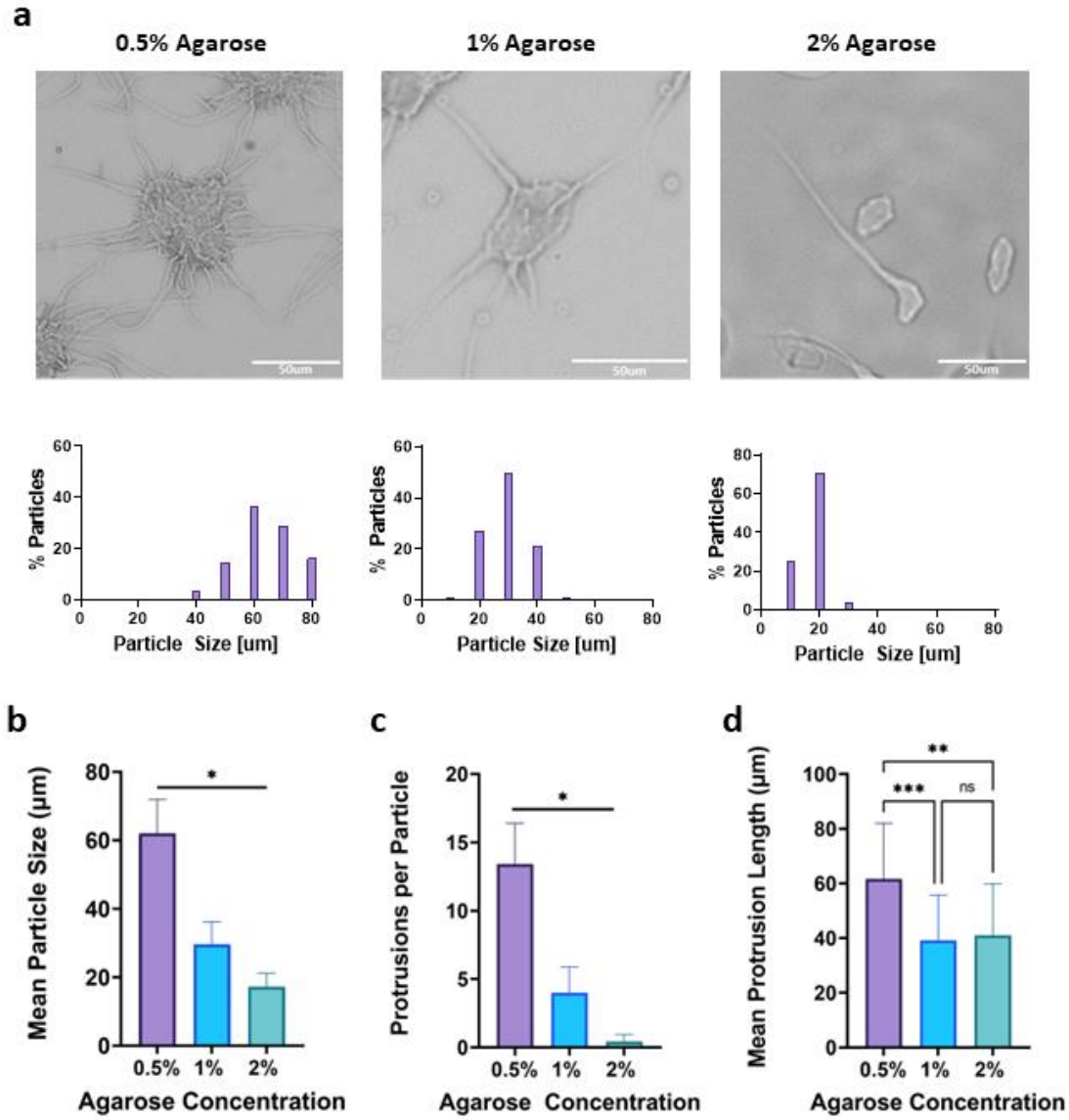

Figure 1: a) Sheared agarose particles created at three different polymer concentrations (0.5%, 1% and 2%), including size distribution analysis. **b)** Quantification of mean particle size for each agarose concentration (* indicates differences are statistical significant, $p<0.05$, one-way ANOVA). **c)** Quantification of mean protrusion number per particle across agarose concentrations (* indicates differences are statistical significant, $p<0.05$, one-way ANOVA). **d)** Quantification of protrusion length across agarose concentrations (**$p<0.01$ and *** $p<0.001$ indicate significant difference compared with 0.5% particles, ns = not significant)

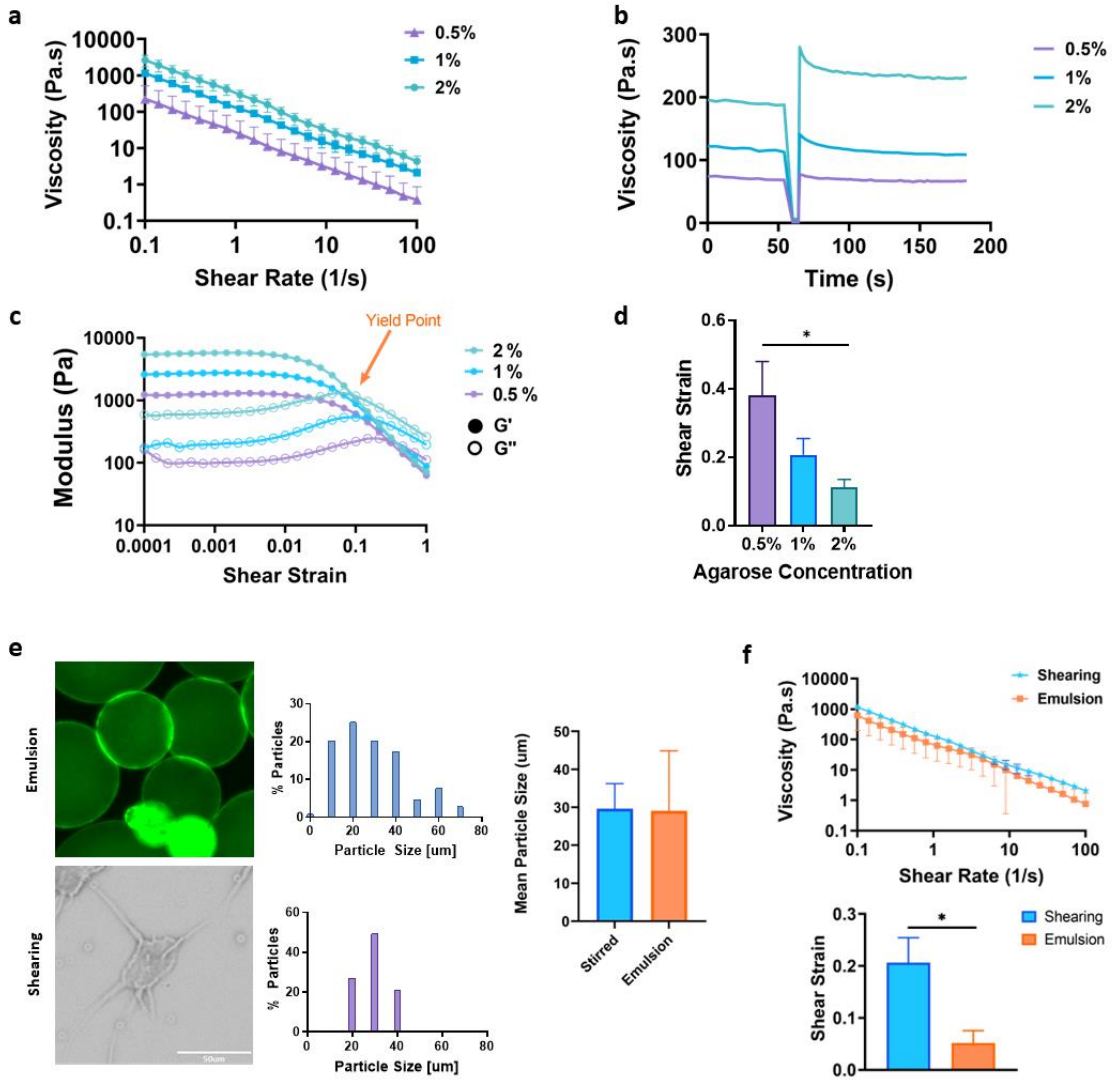

Figure 2: a) Viscosity measurements at increasing shear rates for jammed agarose particles. **b)** Thixotropic test to measure viscosity during one cycle of low (0.01) and high strain (0.1), followed by recover to low strain. **c)** Storage and loss modulus measurements for the different agarose concentrations at increasing shear strain, yield point is defined as region where loss modulus increases above storage modules (elastic to viscous transition.) **d)** Quantification of yield point across all agarose concentrations (* indicates statistical significance with $p<0.05$, one-way ANOVA). **e)** Comparison of agarose particles (1%) created using the shearing and a conventional emulsion method, including quantification of particle size distributions and mean size. **f)** Rheological comparison of shear-thinning and yielding behaviour (derived from storage and loss modulus crossover in strain sweep) in spherical (emulsion method) and non-spherical particles (shearing method) (* indicates statistical significance with $p<0.05$, student t-test). (All data mean ± sd, n=3)

An important consideration when designing granular support hydrogels for bioprinting is the particle packing density. To test how packing density could influence rheological properties we produced granular hydrogels with varied packing density by first forming gels with a destiny of 100% using centrifugation, and the subsequently diluting the particles to 80% and 60%. As packing density decreased from 100% to 60%, viscosity decreased for all particle morphologies. (Fig 3a). Interestingly, there was an interdependence on particle morphology and density, as more spherical particles (2% agarose) were found to have increased viscosity at the 100% packing density, but then this affect was reversed at 60% packing density (Fig 3b). This inverse relationship may be due to protrusions maintaining particle-particle interactions at lower packing densities where there is increased fluid phase between the particles.

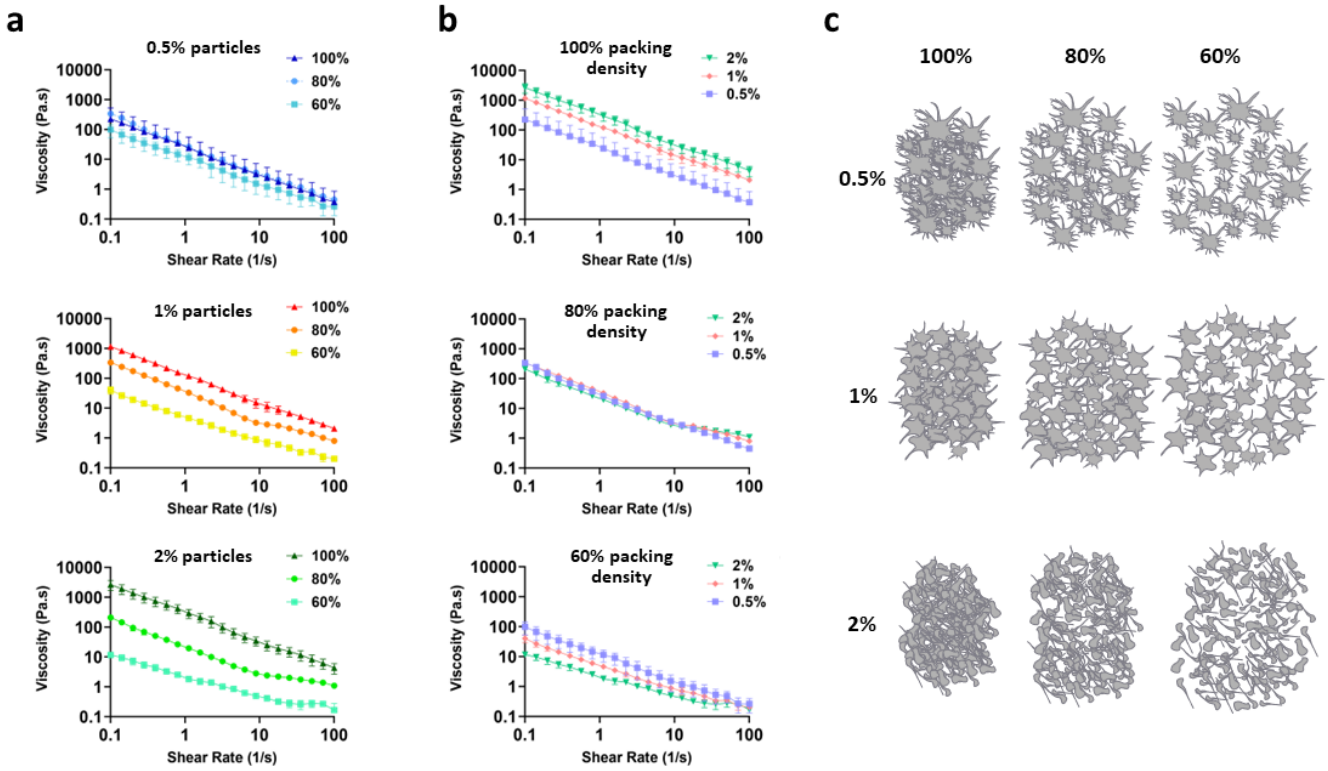

Figure 3: Rheological characterisation of shear-thinning properties in support hydrogels with varied **(a)** packing density and **(b)** agarose concentration. **(c)** Schematics of jammed systems for agarose particles with different agarose concentration (and morphology) and packing densities

Characterizing print quality in granular support hydrogels with varied particle morphology and density

Next, we focused on characterizing how the rheological properties of the support hydrogel could influence print quality during embedded printing. To do this, we developed assays that captured key aspects of the embedded printing process (Fig 4). First, we quantified the width of extruded filaments in the support bath which gives a measure of printing resolution (Fig 4b). Due to their shear rate dependent viscoelastic properties of granular hydrogels, we performed this assay across different print speeds. The ability to maintain print quality and consistency through direction change is an important consideration during embedded printing. To assess this behaviour, we next characterized the filament diameter during directions changes at the entry and turning points (Fig 4c). Another important consideration during embedded printing, is potential disruption of a printed structure due to the subsequent printing of another structure nearby in the support hydrogel. This has important implications for the ability of the printer

to accurately transpose a structure from the design files into the support bath. The rheological properties of the support hydrogel will play an important role in this process as the support must be dislodged as a new material is laid down during printing. We developed two assays for quantifying disruption effects - one for disruption though parallel motion of the printing nozzle, and the other for disruption from perpendicular motion. Disruption due to perpendicular motion is assessed by depositing two lines at a right angle at a set distance from each other, and then measuring variances in the prescribed (g-code) and actual distance between the lines (Fig 4d). Disruption due to parallel printing uses the same assay structure described for the direction change assay, followed by comparing the filament diameter before and after an additional filament was deposited adjacently (Fig 4c). Each measure of print quality was assessed across support hydrogels with varied particle shape and packing density.

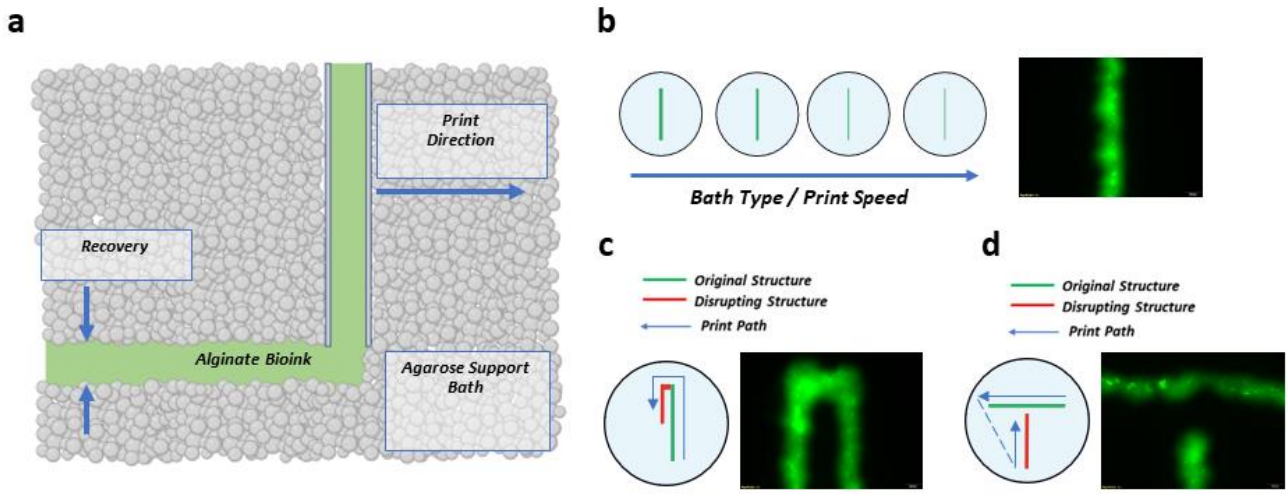

Figure 4: a) Illustration of the support bath bioprinting process. **b)** Linear resolution assay -a straight line is printed and print speed/support bath are varied. The resolution, represented as the width of the printed filament, is observed. Parallel (**c**) and perpendicular (**d**) disruption assay demonstrating sequence of print paths along with representative results.

Particle morphology did not significantly affect print quality during extrusion of simple linear beams, and no significant differences in print resolution were observed between support baths created using agarose particles with concentrations of 0.5%, 1% or 2% (all 100% packing density) (Fig 5 b i). As expected, the resolution of extruded filaments decreased with increasing speed across all support hydrogel compositions (Fig 5 b ii). In the direction change assays we first measured the filament width at the entry and at the corner of the print path to assess consistency during complex paths. We subtracted these measurements to calculate the filament width differences (linear versus corner region), and we then defined the print quality as the ratio between the filament width in the linear and corner region (print quality of 1 being ideal). Interestingly, we observed more consistent print results for 0.5% particles across all packing densities (Fig 5 b ii, iii). Notably, the print quality measurements were significantly lower in support baths created using 2% particles, and these effects were exacerbated at 60% packing density where the print path was undistinguishable (Fig 5 a). Filament precision during this part of a print cycle is vital consideration that will impact the quality of the printed structure.

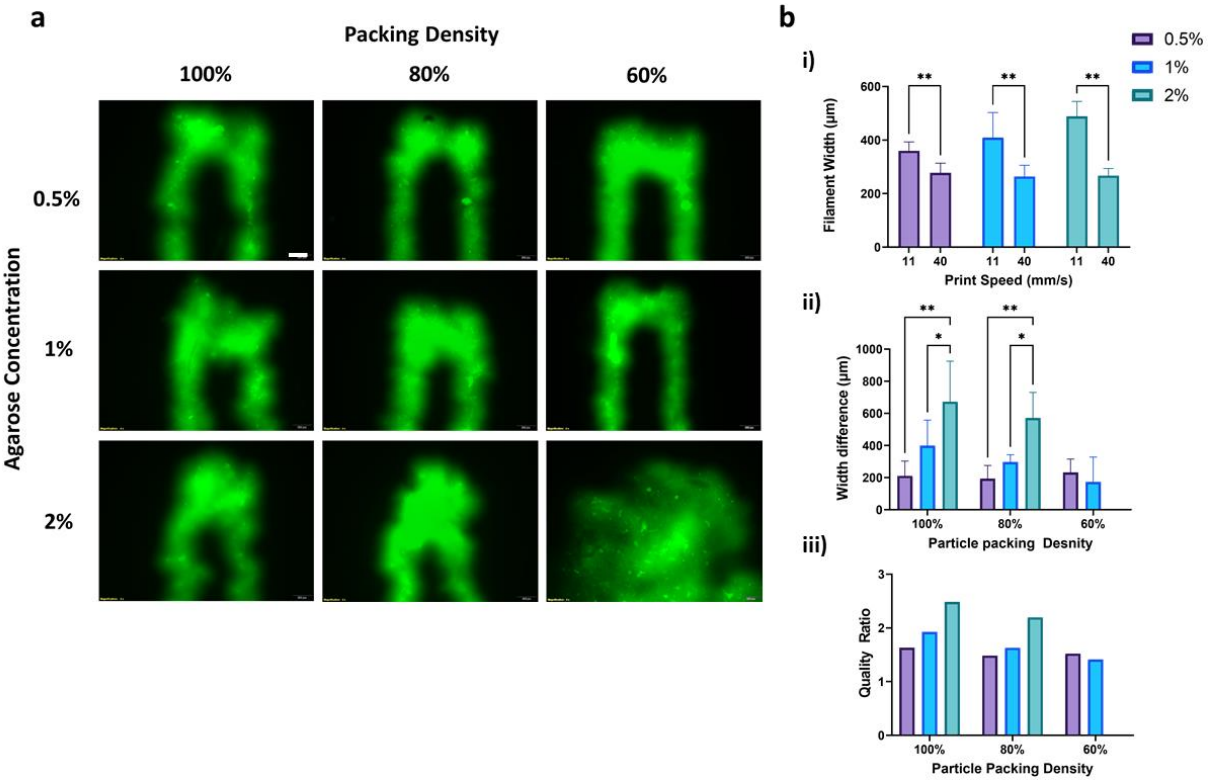

Figure 5: a) Representative results of direction change print assay across all agarose concentrations and particle packing densities (scalebar 200µm). **b) i)** Measurements of linear filament width during printing for each agarose concentrations at both 11mm/s and 40mm/s nozzle translation speed. **b) ii)** Quantification of width difference during direction change print quality assay at different agarose concentrations and particle packing densities (measured by quantifying the difference in filament width between the linear and corner portions of the structure). **(b) (iii)** Quantification of quality ratio at different agarose concentrations and particle packing densities (filament width at corner/filament width at entry point). (All data mean ± sd, n=3, * indicates statistical significance with $p<0.05$, ** indicates statistical significance with $p<0.01$, one-way ANOVA)

Perpendicular co-printing disruption assays demonstrated similar trends, with the least disruption (and therefore highest quality) occurring in baths created using 0.5% particles (Fig 6 a). Similarly, increases in the disruption of the adjacent filaments were observed at lower particle packing densities (Fig 6 a). The lowest levels of disruption were observed in support hydrogels with 100% packing density containing 0.5% agarose particles (high protrusion number) (Fig 6 a). This result correlates with the higher yield points observed in during the strain sweeps (Fig 2 d). There was also a parallel disruption effect which appeared to cause a narrowing of disrupted filaments (those with another parallel line printed 1 mm away) compared with undisrupted filaments (those printed alone) (Figure 6 b). This effect occurred across all support hydrogel formulations, but significant differences were not observed between groups (Fig 6 b). Next, we used simple linear regression to assess if correlations existed between the print quality measurements and corresponding rheological characteristics (Fig 7). We noted a significant correlation (slope significantly non-zero) between print quality and three rheological characteristics: viscosity, storage modulus and loss modulus. R-squared values for each have been determined as 0.57 (viscosity), 0.77 (loss modulus) and 0.67 (storage modulus) (Fig 7 a-c). No

significant correlation between other print and rheological characteristics were found.

Consistent improvements in print quality were observed for the 0.5% agarose particles that were larger in size and presented a distinct morphology with multiple protrusions connected to the central body of the particle. For example, across all packing densities these particles were able to maintain the highest filament consistency during direction changes (Fig 5 b ii). Similarly, we observed reduced disruption of pre-existing filaments during extrusion for these particles (Fig 6 a). Support hydrogels produced using these particles possessed a lower viscosity, and the regression analysis pointed to improved print quality with lower viscosity (Fig 7 a). Higher viscosity will likely cause increased levels of peripheral material flow in the support hydrogel during nozzle translation, which would explain the disruption effects we observed. The higher yield points (strain value where an elastic to viscous transition occurs) observed for 0.5% particle hydrogels may also reduce peripheral support hydrogel flow during ink extrusion (Fig 2 d, f). This effect is potentially due to the increased number of protrusions causing particle entanglement in the interstitial phase. Note, a minimum viscosity is required to support the embedded printing process, as we observed complete failure of the printing process for 2% particles at 60% packing density, which possessed the lowest viscosity of all formulations.

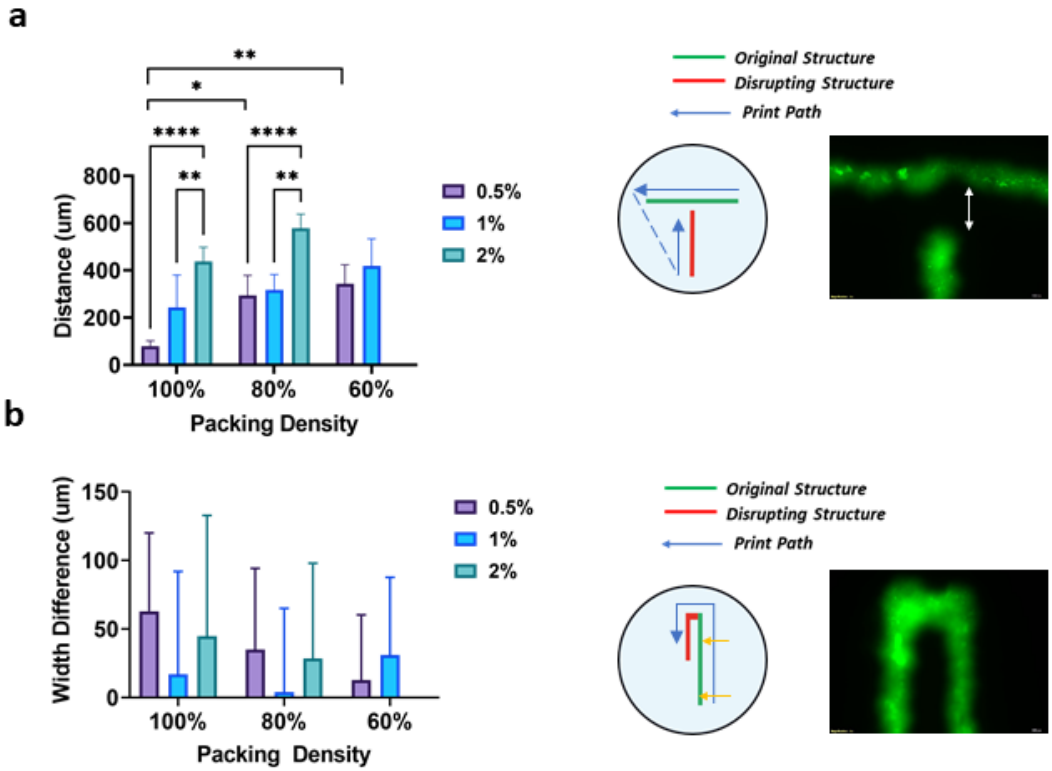

Figure 6: a) Quantification of perpendicular disruption distance in support hydrogels with varied agarose concentration and packing density – distance measured between filaments denoted by white arrow. The g-code file was prescribed to produce a distance of 150µm between the filaments. **b)** Quantification of parallel disruption width difference in support hydrogels with varied agarose concentration and packing density – width difference was measured by quantifying the difference in filament diameter at two locations denoted by the yellow arrows. (All data mean ± sd, n=3, * indicates statistical significance with $p<0.05$, ** indicates statistical significance with $p<0.01$, **** indicates statistical significance with $p<0.0001$, one-way ANOVA)

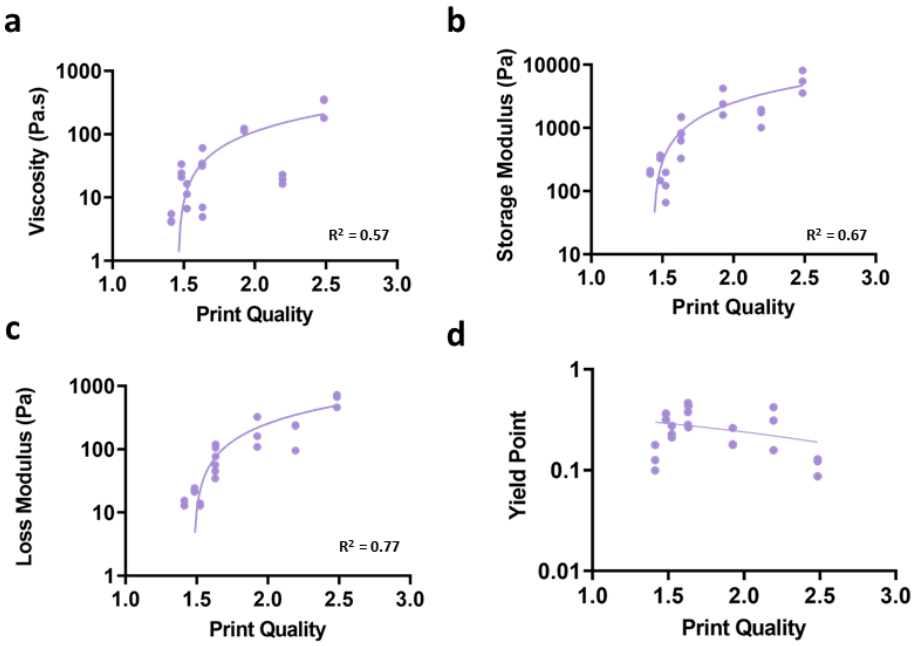

Figure 7: Support hydrogel viscosity **(a)**, loss modulus **(b)** and storage modulus **(c)** correlate with print quality – with r-squared values of 0.57, 0.77 and 0.67 respectively. Print quality measurements are taken from the direction change assays (Fig 5 a iii). **(d)** No correlation was observed between yield point and print quality.

Limitations of this study include the challenges of fully decoupling the mechanical and morphological properties of the particles. For example, the stiffness of the agarose particles will be lower for 0.5% particles, which as well as the particle morphology, will also influence rheological properties. However, we did observe significant differences in the rheological properties of the particles produced with the same polymer concentration produced using an emulsion (spherical particles) and shearing methods (particles with protrusions) (Fig 2 e, f). It was also not possible to fully decouple the influence of particle size and morphology, as these properties cannot be independently controlled using the shearing method. Despite these limitations, significant differences in print quality outcomes were observed across the parameters we explored, and pointed to the benefits of support hydrogels with a low viscosity but a high yield point, which to the best of the author's knowledge has not been reported before. Further, our results highlight how irregular particle morphologies that increase particle-particle interactions can be used to engineer such properties in granular support hydrogels.

Methods

Bioink and support hydrogel fabrication

Alginate was used as a bioink throughout. The ink was created by dissolving alginic acid powder (alginic acid sodium salt from brown algae, Sigma Aldrich) in phosphate buffered solution (PBS) at 7wt%. Fluorescein isothiocyanate (FITC) (Sigma Aldrich) was added at 0.3mg/ml to enable fluorescent imaging. Agarose particles were used to form the support bath. Agarose supports were created using two methods: shearing and emulsion. For the shearing method, agarose powder (Type I, low EEO, Sigma Aldrich) was dissolved in PBS in the required ratio at the required concentration (0.5%, 1%, 2%), followed by heating in a microwave for 1 minute to create a homogenous solution. Next, the melted agarose solution was placed on a magnetic stirrer at 700rpm for 3 hours while cooling to ambient room temperature. This method gives rise to a suspension of agarose particles as the polymer cools under shearing[16,17,19]. To create spherical particles, a batch emulsion method was used. For this method, the melted agarose solution was instead added to mineral Oil (Sigma Aldrich) containing surfactant Span80 (Sigma Aldrich) at a ratio of 98:2. The agarose was heated to

>85° before adding, and the Oil/Span80 mixture was heated to 60° and stirred at 800rpm. Using a pipette warmed to 60°, 1ml of heated agarose/PBS mixture was added to 10ml of oil/Span80. Stirring was continued until the oil/span80 cools to ambient temperature (<30°), typically within 30minutes. Stirring rate optimization was performed to ensure the spherical particles had the same mean diameter as the particles produced using the shearing method. Support baths consist of jammed agarose particles created using either the stirring method or the emulsion method. In order to create a jammed system, agarose particles are placed in a centrifuge and spun at 2000g for 5 minutes at 22°, and excess PBS was then removed. The particles remaining are then in a jammed form with 100% packing. Dilution of the 100% system with PBS was used to create support hydrogels with 80% and 60% packing density. The jammed particles (500mg) were then added to a glass bottom dish for embedded bioprinting and subsequent imaging.

Rheological characterization

The viscoelastic hydrogels used were characterized by shear rheometry (TA Instruments AR2000, cone and plate geometry). Viscosity sweep, strain sweep and thixotropic analyses was carried out to assess key parameters relevant to embedded bioprinting. This testing was performed on 0.5%, 1% and 2% stirred agarose particles in 100%, 80% and 60% packing density jammed systems. Emulsion particles at 1% concentration were similarly analyzed at 100% packing density. Viscosity sweeps were performed in the shear stress range of 0.1-100 1/s. To characterize storage modulus (Pa) and loss modulus a shear strain sweep from 0.0001-1 was used. The yield point of the material is the point at which storage and loss modulus intersect. Finally, three interval thixotropic analysis was performed to assess structural regeneration or self-healing. To do this, low shear was applied for 60 seconds (0.01), followed by high shear for 5 seconds (0.1) and low shear for 120s in the third interval (0.01). Viscosity of the material was recorded through each strain cycle.

Microscopy analysis

An inverted fluorescent microscope (Nikon PV1000) was used for all microscopy. Brightfield mode was used to image the agarose particles post fabrication. Fluorescent imaging was used to assess the printed alginate bioink (containing fluorescein isothiocyanate – FITC, 0.3mg/ml) within the support bath. All image analysis is performed in Image-J.

Bioprinting workflow

An allevi 2 bioprinter was used for all bioprinting, in conjunction with an air compressor to provide pneumatic pressure. Print designs were created in Autodesk Inventor and then exported to an STL format file. STL files were then converted into a computer numerical code language (g-code) via a slicing software (Repetier-Host). All g-code used was manually checked to ensure settings such as print speed were accurately assigned. For the 7% alginate bioink the following optimized settings were used: temperature 30°; pressure 5psi; print speed 11mm/s (40mm/s also used) and nozzle diameter 30 gauge or 0.312mm.

We developed assays to focus on three aspects of print quality during embedded printing: filament resolution, direction change and co-printing disruption. Assays were performed to provide quantitative data on each of these aspects across support bath material concentration and particle packing density. For the linear resolution assay, a line (in the form of a cuboid filament 10mmx0.15mmx0.15mm) was printed into a support bath (Fig 4 b). The width of the filament was measured at multiple points along the 10mm length. Ideally, the filament width would be 0.15mm. The mean filament width describes and is the quantifiable measure of the achievable resolution for a given print speed and bath.

The ability to maintain print quality and consistency through direction change is an important parameter for support bath design and selection. In the direction change assay, three connected lines were continuously printed at right angles to each other. First a long 10mm line, then a 1mm line perpendicular to the top of the first line, followed by a 5mm line parallel to the first and perpendicular to the second (Fig 4 c). Images of the three sided top of this structure were taken, and the width of filaments on either side and the top are measured. By dividing the mean top filament width by the mean side filament width, a ratio representing the print quality through direction change is obtained. Ideally both would be 0.15mm and the ratio equal to 1. This is the quantitative measure of print quality through direction change that is presented in the results.

Disruption of a printed structure due to the subsequent printing of another structure was also analyzed. This has important implications for the ability the printer to accurately transpose a structure from the design files to the support bath. Two assays were used here - one for disruption though parallel motion (Fig 4 c) and the other for disruption from perpendicular motion (Fig 4 d). Disruption due to parallel printing uses the same assay structure described for the direction change assay (Figure 4 c). The filament width in the first half of the 10mm line (with no parallel line printed) is the undisrupted width. The filament width of the top half of the 10mm line has a second line printed in parallel 1mm away - this is the disrupted width. By comparing the difference in the filament width observed, a measure for parallel disruption is obtained. Ideally, both would be the same width. Perpendicular width is assessed by printing a 10mm line again, followed by a 5mm line printed perpendicular to the midpoint of the 10mm line (Fig 4 d). This second line begins 5.15mm away from the first and ends 0.15mm away. The distance from this finish point of the print to the first line is measured. Without any disruption this should be 0.15mm.

Acknowledgements

This publication has emanated from research supported in part by a grant from Science Foundation Ireland and is co-funded under the European Regional Development Fund under Grant number 13/RC/2073_P2.

Author Contributions

Conceptualization and design, G.B., and A.D.; Execution of experiments G.B.; Writing, review, and editing, G.B., and A.D.; Supervision, A.D. All authors critically reviewed and approved the final manuscript.

Declaration of interest

The authors declare no competing interests.

References

1. Malda, J. *et al.* 25th Anniversary Article: Engineering Hydrogels for Biofabrication. *Adv. Mater.* **25**, 5011–5028 (2013).
2. Ozbolat, I. T. & Hospodiuk, M. Current advances and future perspectives in extrusion-based bioprinting. *Biomaterials* **76**, 321–343 (2016).
3. Hospodiuk, M., Dey, M., Sosnoski, D. & Ozbolat, I. T. The bioink: A comprehensive review on bioprintable materials. *Biotechnol. Adv.* **35**, 217–239 (2017).
4. McCormack, A., Highley, C. B., Leslie, N. R. & Melchels, F. P. W. 3D Printing in Suspension Baths: Keeping the Promises of Bioprinting Afloat. *Trends Biotechnol.* **38**, 584–593 (2020).
5. Highley, C. B., Rodell, C. B. & Burdick, J. A. Direct 3D Printing of Shear-Thinning Hydrogels into Self-Healing Hydrogels. *Adv. Mater.* **27**, 5075–5079 (2015).
6. Zhang, Y. *et al.* 3D printed collagen structures at low concentrations supported by jammed microgels. *Bioprinting* **21**, e00121 (2021).
7. Morley, C. D. *et al.* Quantitative characterization of 3D bioprinted structural elements under cell generated forces. *Nat. Commun.* **10**, 1–9 (2019).
8. Daly, A. C., Critchley, S. E., Rencsok, E. M. & Kelly, D. J. A comparison of different bioinks for 3D bioprinting of fibrocartilage and hyaline cartilage. *Biofabrication* **8**, 45002 (2016).
9. Lee, A. *et al.* 3D bioprinting of collagen to rebuild components of the human heart. *Science* **365**, 482–487 (2019).
10. Bhattacharjee, T. *et al.* Writing in the granular gel medium. *Sci. Adv.* **1**, 4–10 (2015).
11. Hinton, T. J. *et al.* Three-dimensional printing of complex biological structures by freeform reversible embedding of suspended hydrogels. *Sci. Adv.* **1**, e1500758 (2015).
12. Daly, A. C., Riley, L., Segura, T. & Burdick, J. A. Hydrogel microparticles for biomedical applications. *Nat. Rev. Mater.* **5**, 20–43 (2020).
13. Jeon, O. *et al.* Individual cell-only bioink and photocurable supporting medium for 3D printing and generation of engineered tissues with complex geometries. *Mater. Horiz.* **6**, 1625–1631 (2019).

14. Moxon, S. R. *et al.* Suspended Manufacture of Biological Structures. *Adv. Mater.* **29**, (2017).
15. Cooke, M. E. & Rosenzweig, D. H. The rheology of direct and suspended extrusion bioprinting The rheology of direct and suspended extrusion bioprinting. **011502**, (2021).
16. Ghebremedhin, M., Seiffert, S. & Vilgis, T. A. Physics of agarose fluid gels: Rheological properties and microstructure. *Curr. Res. Food Sci.* **4**, 436–448 (2021).
17. Norton, I. T., Jarvis, D. A. & Foster, T. J. A molecular model for the formation and properties of fluid gels. *Int. J. Biol. Macromol.* **26**, 255–261 (1999).
18. Yan, Y. *et al.* Mechanical characterization of agarose micro-particles with a narrow size distribution. *Powder Technol.* **192**, 122–130 (2009).
19. Prendergast, M. E. & Burdick, J. A. Computational Modeling and Experimental Characterization of Extrusion Printing into Suspension Baths. *Adv. Healthc. Mater.* **11**, 1–14 (2022).
20. Mirdamadi, E., Muselimyan, N., Koti, P., Asfour, H. & Sarvazyan, N. Agarose Slurry as a Support Medium for Bioprinting and Culturing Freestanding Cell-Laden Hydrogel Constructs. *3D Print. Addit. Manuf.* **6**, 158–164 (2019).
21. Senior, J. J., Cooke, M. E., Grover, L. M. & Smith, A. M. Fabrication of Complex Hydrogel Structures Using Suspended Layer Additive Manufacturing (SLAM). *Adv. Funct. Mater.* **29**, 1904845 (2019).